Available online at www.sciencedirect.com
SCIENCE DIRECT®
International Journal of Heat and Fluid Flow 27 (2006) 123–134
International Journal of HEAT AND FLUID FLOW
www.elsevier.com/locate/ijhff

MicroPIV measurements of turbulent flow in square microchannels with hydraulic diameters from 200 μm to 640 μm

Hao Li, Michael G. Olsen *

Department of Mechanical Engineering, Iowa State University, 3025 H.M. Black Engineering Building, Ames, IA 50011, USA

Received 5 August 2004; accepted 18 February 2005
Available online 23 May 2005

Abstract

Microscopic particle image velocimetry (microPIV) experiments were performed on square polydimethylsiloxane (PDMS) microchannels with hydraulic diameters ranging from 200 μm to 640 μm and for Reynolds numbers ranging from 200 through 3971. Deionized water mixed with fluorescent seed particles was used as the working fluid. There was no evidence of early transition to turbulence, with transition observed at Reynolds numbers between 1718 and 1885 for the different sized microchannels. The 200 μm microchannel structurally failed before fully turbulent flow was reached, but for the other microchannel geometries studied, the flow was found to become fully turbulent at Reynolds numbers ranging from 2600 to 2900. The measured fully turbulent $\langle u' \rangle / u_{\max}$ velocity fluctuations agreed well with results for turbulent duct flow for the 320 μm, 480 μm and 640 μm microchannels. The measured fully turbulent $\langle v' \rangle / u_{\max}$ fluctuations agreed well with turbulent duct flow results for the 480 μm and 640 μm microchannels, but were 20–40% lower than turbulent duct flow results for the 320 μm microchannel. Similar results were observed in the measured Reynolds shear stresses. Spatial correlations of velocity fluctuations were also measured in the transverse direction, and in the $R_{u'u'}$ spatial correlation results, the 480 μm and 640 μm microchannel results agreed very well with turbulent pipe flow results, but the 320 μm results showed significant differences. The $R_{v'v'}$ correlations were very similar for all three microchannels, with the $R_{v'v'}$ correlations decaying more slowly than the $R_{u'u'}$ correlations.

Keywords: Turbulence; Transition; Microchannel; MicroPIV

1. Introduction

The rapid development of microfluidic microelectromechanical systems (MEMS) has resulted in great interest in the understanding of flow behavior in microchannels due to their importance in such applications as microelectronics cooling (Tuckerman and Pease, 1981), drug delivery, biotechnical analyses, and telecommunication technologies (Henning, 1998; Lipman, 1999). The fluid flow characteristics of microchannels are important to the design of microfluidic devices, and thus this topic is of significant importance to the further development of microfluidic MEMS devices. Because of this importance, researchers have been working in this area since the 1980s, and many interesting, yet often times conflicting, results have been reported.

In many previous studies, researchers measured the friction factor or Nusselt number in microchannel flow and compared the results with conventional theory. For example, Wu and Little (1983) measured the friction factors of gas flow (nitrogen, hydrogen, and argon) through etched glass and silicon microchannels with hydraulic diameters ranging from 45.46 μm to 83.08 μm. Their results suggested an early onset of transition around $Re = 350$, far from the conventional macroscale transitional Reynolds number of 1800–2300. They also measured abnormally high values of friction factor and attributed this to the large relative roughness

* Corresponding author. Tel.: +1 515 294 0073; fax: +1 515 294 3261.
E-mail address: mgolsen@iastate.edu (M.G. Olsen).

0142-727X/$ - see front matter © 2005 Elsevier Inc. All rights reserved.
doi:10.1016/j.ijheatfluidflow.2005.02.003

Nomenclature

Latin and Greek Characters

d	the depth of microchannels (μm)
d_e	the image diameter of particles (μm)
D	diffusivity (m^2/s)
D_h	the hydraulic diameter of microchannels (μm)
d_p	particles diameter (μm)
d_s	the diameter of the diffraction-limited point spread function (μm)
$f^{\#}$	focal number (–)
L	length of turbulent structure (μm)
M	magnification (–)
NA	numerical aperture (–)
R	correlation coefficient (–)
Re	Reynolds number (–)
T	fluid temperature (K)
u	longitudinal velocity in microchannel (m/s)
u'	fluctuation of instantaneous velocity u (m/s)
v'	fluctuation of instantaneous transverse velocity (m/s)
W	width of the microchannel (μm)
y	transverse position (μm)
β	constant, 3.67 (–)
Δt	time period between two laser pulses (μm)
Δy	displacement in transverse direction (μm)
ε	relative measurement uncertainty (%)
ε_s	microchannel surface roughness (μm)
μ	fluid absolute viscosity (kg/m s)

Mathematical symbol

$\langle\,\rangle$	ensemble averaging value

Subscripts

center	velocity at the center region of the channel
max	maximum value

of the etched channels. Peng et al. (1994), Peng and Peterson (1996) measured the friction factor of water flow through rectangular stainless steel microchannels with hydraulic diameters of 0.133–0.367 mm and aspect ratios of 0.333–1. Their results showed transition occurring at $Re = 200-700$ and fully turbulent flow also occurring at lower Reynolds numbers than macroscale channels. Mala and Li (1999) investigated water flow through fused silica and stainless steel microtubes with diameters ranging from 50 to 254 μm, and based on observations of the nonlinear relationship between pressure gradient and the volumetric flow rate at $300–500 \leqslant Re \leqslant 1000–1500$ concluded that early transition was occurring. They also found rough agreement between the friction factor of experimental data and conventional theory at low Reynolds numbers, but, as Reynolds number was increased, the experimental friction factor showed a significant increase from macroscale results (Qu et al., 2000), a phenomenon they attributed to surface roughness. Pfund et al. (2000) detected the turbulent transition by friction factor and flow visualization. Their test channels had high aspect ratios and depths ranging from 128 μm to 521 μm. The Reynolds numbers investigated were from 60 to 3450. Slightly early "sudden, but not discontinuous" transition was observed and friction factor values significantly greater than those predicted by macroscale correlations were measured. Other researchers claimed to observe early transition, but measured friction factors that agreed well with macroscale correlations. For example, Gui and Scaringe (1995) investigated flow in microchannels with hydraulic diameters up to 388 μm and found transition at $Re = 1400$, but found friction factors that agreed well with the conventional theory. Wu and Cheng (2003) found the onset of transition at $Re = 1500$ for water flow in smooth, trapezoidal silicon microchannels with hydraulic diameters in the range of 25.9–291.0 μm, but the experimental data matched well with the analytical solution for incompressible, fully developed, laminar flow under a no-slip boundary condition. One common point in many of these studies is that researchers who found early laminar-turbulent transition concluded that the relatively high surface roughness was one of the major reasons (Qu et al., 2000; Guo and Li, 2003a,b; Sabry, 2000; Toh et al., 2002).

However, there are also researchers whose results on transition agreed well with conventional predictions even with the same magnitude of channel surface roughness (1–2%) as researchers mentioned before. For instance, Hegab et al. (2001, 2002) performed experiments on single-phase flow in microchannels with hydraulic diameters ranging from 112 μm to 210 μm and aspect ratios from 1.0 to 1.5. They reported transition between $Re = 2000–4000$ and friction factor results that were slightly lower than the conventional predictions. Qu and Mudawar (2002) studied the fluid flow characteristics of a microchannel heat sink with dimensions of 231 μm × 713 μm for Reynolds numbers between 39 and 1672. They found no evidence of early transition, and the measured pressure drop showed good agreement with corresponding numerical predictions. Judy et al. (2002) measured frictional pressure drop of fluid flow in microtubes with hydraulic diameters between 15 μm and 150 μm for three different fluids (water, methanol, isopropanol), two different tube materials

(fused silica, stainless steel), and two different tube cross-section geometries (circular, square) and found no "distinguishable" deviation from macroscale viscous flow theory. Chung et al. (2002) performed experiments on single-phase flow in a 100 μm capillary tube. Good agreement was observed when the measured friction factor was compared with the conventional theory for deionized water flow, although surface roughness was not considered. The measured velocity also matched the theoretical profile for laminar flow in a circular microchannel. For gas flows, the compressibility effect was found to be important to match the experimental data with theory.

The previously mentioned experiments applied pressure drop measurements in their investigations of microfluidic flow. However, since discrepancies exist in the existing literature on microfluidic flow transitional behavior (Celata et al., 2004), some researchers have attempted to clarify it using a relatively new experimental technique, microscopic particle image velocimetry (microPIV) (Santiago et al., 1998; Meinhart et al., 1999; Olsen and Adrian, 2000a; Devasenathipathy et al., 2003). Because of its advantage as a non-invasive measurement technique in microscale flow systems, microPIV has been widely used in researching many different microscale flows (Stone et al., 2002; Klank et al., 2002; Kim et al., 2002). Using microPIV, Zeighami et al. (2000) performed an experimental investigation on transition in a silicon microchannel with dimensions 150 μm × 100 μm × 1 cm. The repeatability of the velocity data and the motion of seed particles perpendicular to the measurement plane were taken as the criteria to distinguish laminar and turbulent flow. Using this criteria, early transition at $Re = 1200-1600$ was observed. However, in this study, the particle seed density was not sufficient for Reynolds stresses to be measured or for turbulent flow structures to be observed. Lee et al. (2002) studied flow up to $Re = 2900$ in a rectangular microchannel of aspect ratio 2.65 and hydraulic diameter 380 μm. In their work, the deviation of velocity profiles and a broadening of the microPIV cross-correlation signal peak with turbulence intensity was used to define transition at $Re = 2900$. Sharp and Adrian (2004) performed a detailed set of pressure drop and microPIV experiments on transitional flow in microtubes. Round glass microtubes with diameters between 50 and 247 μm were used along with working fluids of different polarities. In their microPIV experiments, fluctuations of the centerline velocity were taken as indicators of the transition to turbulence. In the laminar regime, centerline velocity fluctuations of around 1% (due to experimental noise) were observed. However, at higher Reynolds numbers, the centerline velocity fluctuations increased, and the first abrupt increase of the rms value of centerline velocity was taken as the onset of transitional flow. Using this definition, transition was observed between $1800 < Re < 2200$, and thus they concluded that anomalous transition did not occur.

The present work uses microPIV to obtain instantaneous velocity field data for flow through square microchannels with hydraulic diameters ranging from 200 μm to 640 μm and aspect ratios close to 1. The particle seeding was dense enough that Reynolds stresses could be measured throughout the microchannel. The measured Reynolds stresses are then compared with classical results for macroscale ducts. Finally, spatial correlations of velocity fluctuations are calculated and reported.

2. Microchannel fabrication

The straight microchannels used in the present experiments were fabricated using PDMS replica molding (Anderson et al., 2000; Jo et al., 2000). A brief summary of the fabrication process follows (greater detail of the fabrication process can be found in Li et al. (2005)). Fig. 1 summarizes the fabrication procedure graphically. The channel molds were made from patterned negative photoresist (SU-8 2100, MicroChem Corp., Newton, MA) on a silicon wafer (100 mm diameter, Montco Silicon Technologies, Inc, Spring City, PA). A coating of

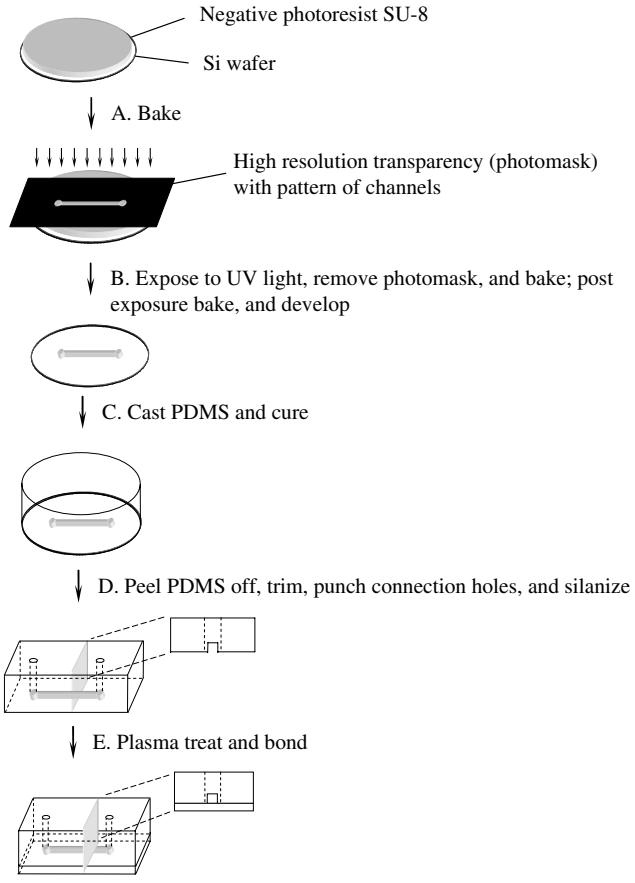

Fig. 1. Summary of the microchannel fabrication technique.

the photoresist was spun on the silicon wafer, and select regions of the coated wafer were exposed through a transparency film to ultraviolet light. The photoresist was then developed resulting in a mold of the microchannel geometry in relief. Polydimethylsiloxane (PDMS) elastomer (Sylgard(R) 184 Silicone Elastomer Kit, Dow Corning, Midland, MI) was then cast on the mold and baked. Finally, the two halves of the microchannel are plasma treated and bonded to form the finished microchannel.

Microchannels were fabricated with four different hydraulic diameters and with aspect ratios very close to 1. The different widths were controlled by varying the design drawings of transparencies, and the different depths were controlled by adjusting the amount of photoresist deposited on the wafer, the spinning speed of spin coater, the baking time, and the exposure time to UV light. Accurate determination of dimensions was essential to obtain reliable data. The optical measurement of the dimensions at various positions along the microchannels, accurate to within ±10 μm, indicated variations between 1.6% and 5%. The final length-averaged dimensions of the four different microchannel geometries were confirmed with a microscope and are listed in Table 1.

The resulting microchannels were then tested for inner surface roughness using Dektak IIA surface profile measuring system (Veeco Instruments Inc., Santa Barbara, CA). Liner surface profiles were taken of the cast PDMS. These measurements were limited, as the profilometer stylus could only be used on the top and bottom surfaces of the channel. For example, for the 320 μm microchannel, the arithmetic average roughness was calculated by the Dektak IIA software to be approximately 24 nm. This results in a relative roughness $\varepsilon_s/D_h \approx 0.000074$.

3. Experimental apparatus and methodology

The experimental system, schematically shown in Fig. 2, consisted of two sub-systems: (i) the flow delivery system; and (ii) the microPIV system. The flow was driven by a micro gear pump and pump head (115 VAC console digital dispensing drive and 0.084 mL/rev suction shoe gear pump head, Cole-Parmer Instrument Co., Vernon Hills, IL) that provided constant flow rates accurate to within ±0.3%. The working fluid was deionized water. Flow from the gear pump passed through the microchannel, then through a digital flowmeter (0–100 mL/min volumetric water flow meter, Cole-Parmer Instrument Co., Vernon Hills, IL), and finally through a fluid reservoir before returning to the gear pump to begin a second cycle. The flowmeter contained a thermocouple so fluid temperature could be carefully monitored during each run. The purpose of the fluid reservoir was to increase the thermal mass of the fluid in the system, so that viscous dissipation did not result in any temperature change of the working fluid (and hence a change in fluid viscosity) during the experimental runs.

Table 1
Geometric parameters of test microchannels

Channel name	W (μm)	d (μm)	D_h (μm)	Aspect ratio (W/d)
200 μm	200	200	200	1.00
320 μm	320	330	325	0.97
480 μm	480	490	485	0.98
640 μm	640	640	640	1.00

The microPIV system is shown in the lower portion of Fig. 2. A double pulsed Nd:YAG laser beam (Continuum, Santa Clara, CA), attenuated to 3 mJ/pulse with a wavelength of 532 nm, was expanded and directed into an aperture in the rear of the microscope. Nine-hundred nanometers diameter fluorescent seed particles (Duke Scientific Co., Palo Alto, CA) were excited by the laser light and emitted light at a peak excitation wavelength of 612 nm. The excited light, filtered by a beamsplitter to remove illuminating and background light, was then imaged through the inverted biological microscope [Nikon model T-300 Inverted Microscope] and an objective lens with a magnification of 20× and a numerical aperture of 0.45. A LaVision Flowmaster 3 camera (Lavision Inc., Ypsilanti, MI) was used to capture the PIV image pairs for cross-correlation analysis.

The concentration of the fluorescent particle solution was prepared such that a sufficient number of seed particles fell within depth of correlation (Olsen and Adrian, 2000a; Bourdon et al., 2004) of each interrogation region that erroneous vector measurements were minimized. In the present experiments, the 20× 0.45 NA objective yields a depth of correlation of 8.3 μm (an alternate definition of depth of correlation by Meinhart et al. (1999) yields a similar result for depth of correlation). Using interrogation windows measuring 28 μm square (for the 200 μm, 320 μm, and 480 μm microchannels) and 56 μm square (for the 640 μm microchannel) and overlapping each interrogation region by 50% yielded spatial resolutions of 14 μm and 28 μm, respectively. Achieving this spatial resolution required a volumetric particle concentration of approximately 0.057%. This volume fraction of seed particles was small enough that any two-phase effects were negligible, and the working fluid could be considered a single-phase fluid.

The experiments were performed at various flow rates corresponding to Reynolds numbers ranging from 200 up to 3971. For each set of experiments, sufficient time was allowed to pass after starting the micro gear pump to allow the flow to reach steady state. For smaller flow rates, it took a longer time to reach a steady state compared to higher flow rates. A multi-pass interrogation scheme with decreasingly smaller window sizes was used

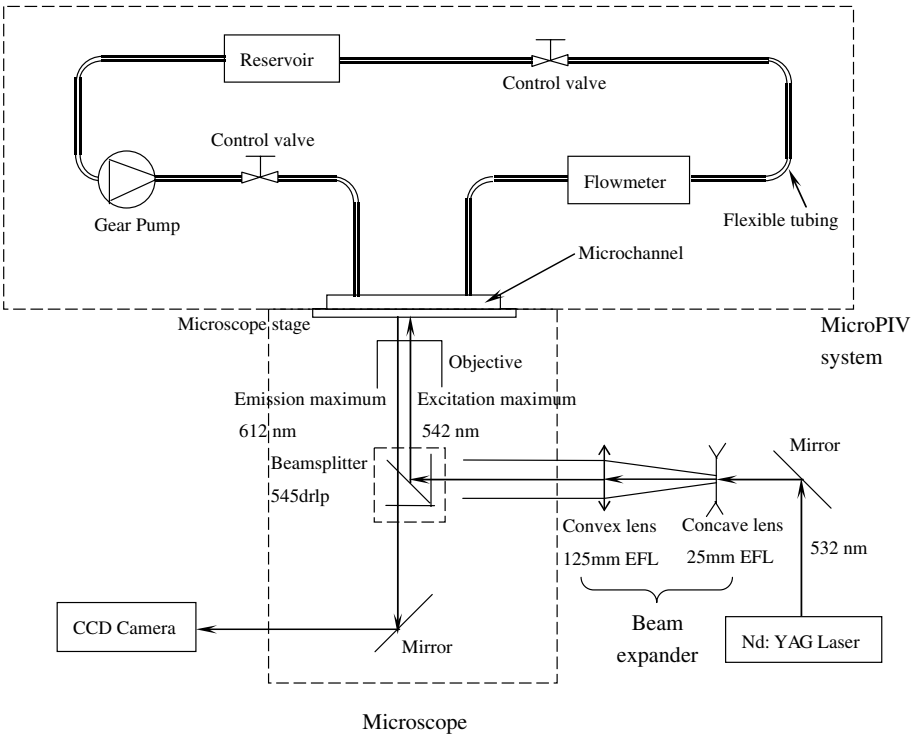

Fig. 2. Schematic of the experimental setup.

in the computation of the vector fields to reach the final 32×32 pixels (for the 200 μm, 320 μm, and 480 μm microchannels) and 64×64 pixels (for the 640 μm microchannel) interrogation windows. The only post-processing performed on the vector fields was the removal of bad vectors. No smoothing of vector fields was performed. The number of velocity fields collected for each Reynolds number ranged from 600 for the lowest, laminar Reynolds numbers to 2000 for the transitional and turbulent Reynolds numbers.

There are two sources of measurement error in the microPIV experiments: errors introduced by random motion of the seed particles due to Brownian motion, and errors implicit in the interrogation of the PIV images. The significance of Brownian motion in the microPIV measurements can be determined by calculating the *Brownian motion coefficient* (Olsen and Adrian, 2000b), defined as

$$\frac{d_e^2}{d_e^2 + 8M^2\beta^2 D\Delta t} \tag{1}$$

where $D = \frac{kT}{6\pi\mu d_p}$ and β^2 is a constant equal to 3.67. For values of the Brownian motion coefficient close to unity, Brownian motion has a negligible effect on the measured velocity. For the 640 μm microchannel at $Re = 1500$, the Brownian motion coefficient is equal to 0.9988, indicating that Brownian motion effects are small. For the smaller microchannels, or at higher Reynolds numbers in the 640 μm microchannel, the Brownian motion effect is even smaller, due to the smaller Δt required for these measurements. Note that the fact that Brownian motion is negligible is not surprising, given the short Δt required for each of the measurements (on the order of 1 μs).

The experimental error due to interrogation of the PIV images can be estimated by assuming that measured particle displacements are accurate to within approximately 1/10th of a seed particle image diameter (Prasad et al., 1992). For the microPIV experiments, the image diameter for a particle in the object plane can be approximated as (Adrian and Yao, 1983)

$$d_e = (M^2 d_p^2 + d_s^2)^{1/2} \tag{2}$$

For the present experiments, $d_e = 1.9$ μm projected back into flow coordinates, meaning that the measured particle displacement in the microPIV experiments should be accurate to within 0.19 μm. For the 200 μm, 320 μm, and 480 μm microchannels experiments, the maximum particle displacement was approximately 7 μm between laser pulses, resulting in an experimental uncertainty of 2.7%, and for the 640 μm microchannel experiments, the particles moved approximately 14 μm, resulting in an experimental uncertainty of around 1.4%. Note that these errors are representative of the high velocity regions in the microchannel since these regions have the largest particle displacements. The experimental error will be higher in the near-wall regions where velocities are lower, as the seed particles in these regions will exhibit smaller displacements between laser pulses. For

example, the experimental error at a location where the local mean velocity is one-half the maximum mean velocity will be twice the earlier reported experimental errors.

The data were taken at locations far enough downstream of the microchannel entrance to ensure fully developed flow and avoid any entrance length effects (Lee et al., 2002). This was verified by taking measurements at different downstream locations and comparing the mean velocity profiles. In all cases, velocity fields were measured along the microchannel midplane by finding the maximal velocity peaks at laminar flow.

4. Results and discussion

The ensemble-averaged streamwise velocity profiles for various Reynolds numbers are presented in Fig. 3, together with the corresponding fully developed laminar analytical solutions for a rectangular pipe (White, 1991). The transverse positions have been normalized by 1/2 of the width of the microchannel, with 0 corresponding to the microchannel centerline and 1 corresponding to the microchannel wall. For the 200 μm microchannel, the comparison shows good agreement between the measured velocity and the laminar solution until $Re = 1708$, with deviations from the laminar solution over most of the profile of less than 1%. The deviation from the laminar profile becomes apparent at $Re = 1792$ where the experimental data become less parabolic with a lower peak value at centerline and higher velocity close the wall, a typical phenomenon of transitional or turbulent flow. Efforts were made to reach higher Reynolds numbers and fully turbulent flow, but unfortunately this size channel kept catastrophically failing due to the high pressure at higher Reynolds numbers. The same measurements were repeated for the 320 μm, 480 μm, and 640 μm microchannels, and the data are shown in Fig. 3(b), (c), and (d), respectively. It is interesting to note that in all of the cases investigated, deviation from the analytical laminar solution occurs before any evidence of transition to turbulence is observed in the plots of velocity fluctuations (Figs. 5 and 6). This behavior is consistent with previous studies of channel and pipe flow at both the macroscale (Wygnanski and Champagne, 1973) and the microscale (Sharp and Adrian, 2004). As Reynolds number is further increased, the measured velocity near the channel centerline deviates further from the laminar prediction and becomes smaller, while the velocity near the channel walls becomes greater, and the measured velocity profiles begin to resemble fully turbulent flow. The changing shape of the mean velocity profiles with increasing Reynolds number is more distinctive in Fig. 4, where the velocity profiles are normalized by the centerline velocity. Fig. 4 also shows the difference between the experimental data and fully turbulent duct flow. At lower Reynolds numbers, the velocity profiles are grouped

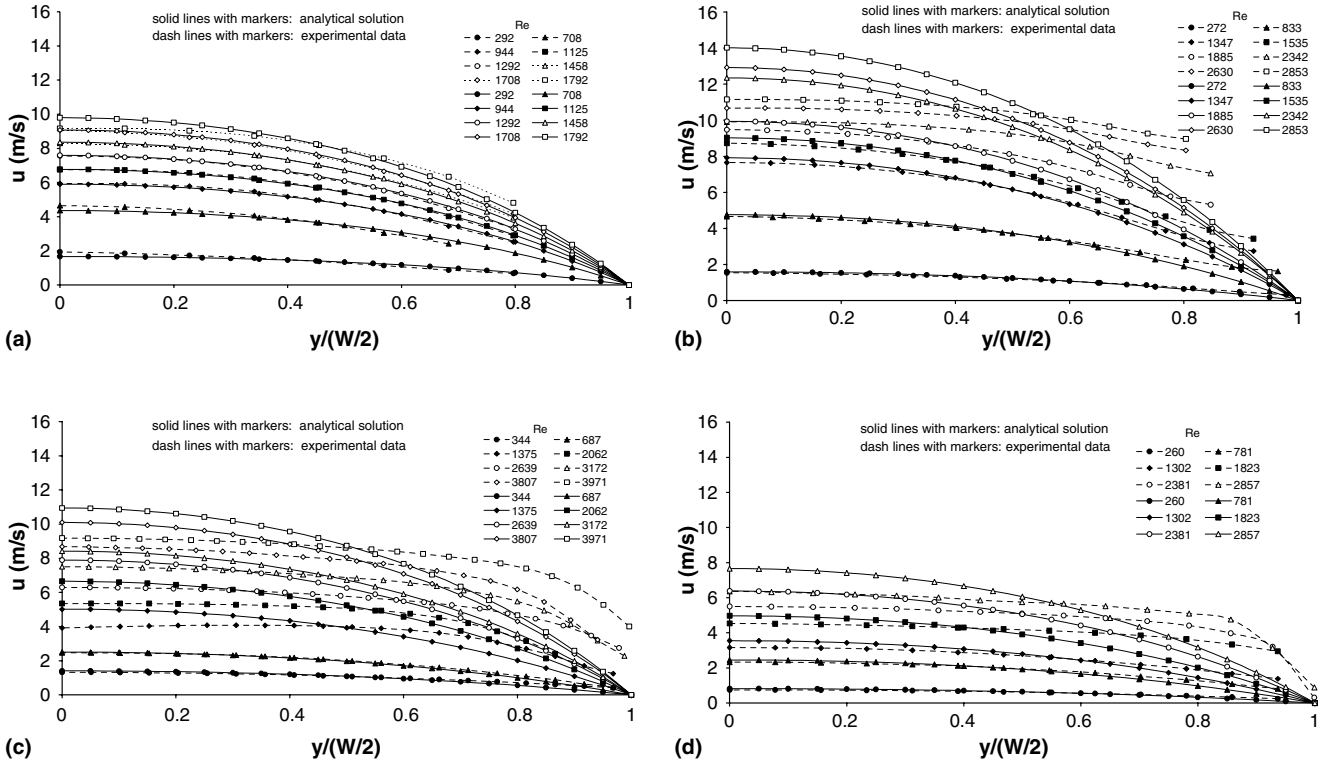

Fig. 3. Mean velocity profiles for the (a) 200 μm, (b) 320 μm; (c) 480 μm, and (d) 640 μm microchannels.

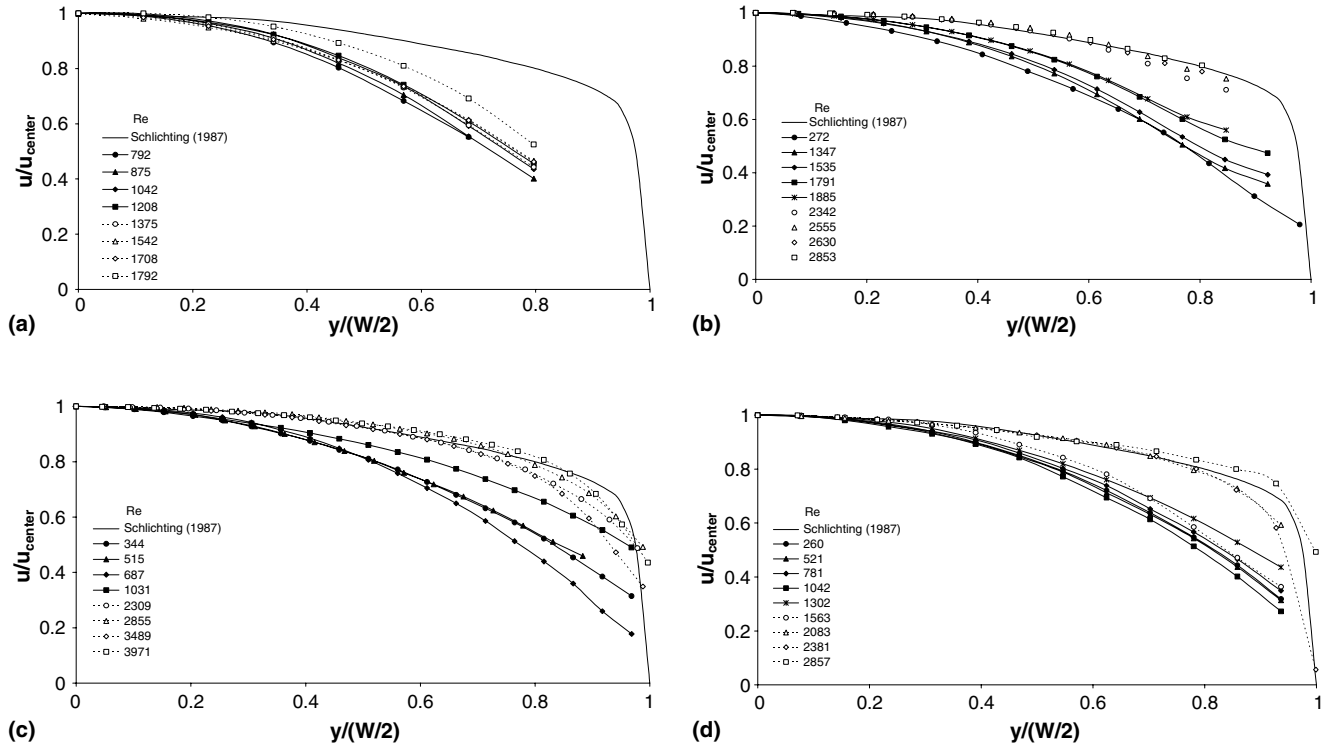

Fig. 4. Normalized mean velocity profiles for the (a) 200 μm, (b) 320 μm; (c) 480 μm, and (d) 640 μm microchannels.

together near the analytical laminar solution. As Reynolds number increases, the velocity profiles first deviate from the laminar solution, and then become grouped together again with only small differences between them (even if there is significant increase of Reynolds number), indicating the onset of fully turbulent duct flow. At the highest Reynolds numbers studied, good agreement is observed between the measured velocity profiles and the velocity profile for fully turbulent macroscale channel flow (Schlichting, 1987) for a smooth channel with maximum velocity 100 cm/s and Reynolds number of 4000 based on hydraulic diameter, suggesting that the microchannel flow has reached a fully turbulent state and presented a good agreement with macroscale experimental results.

In order to quantify the turbulence in the microchannels, velocity fluctuations and Reynolds shear stresses were computed from the microPIV data. Figs. 5–7 show the dimensionless profiles of $\langle u' \rangle / u_{\max}$, $\langle v' \rangle / u_{\max}$, and $-\langle u'v' \rangle / u_{\max}^2$, respectively for each of the microchannels as a function of Reynolds number. For all the microchannels, the measured centerline values of $\langle u' \rangle / u_{\max}$ exhibit a band of overlapped fluctuation values around 1.5% at Reynolds numbers lower than $Re = 1500$, as shown in Fig. 5. The measured fluctuations at these low Reynolds numbers are not evidence of turbulence, but are instead due to the measurement uncertainty in the microPIV experiments.

In their microPIV experiments in microtubes, Sharp and Adrian (2004) defined transition to turbulence based on a significant increase in the measured centerline streamwise velocity fluctuations. Using this definition for transition in the present experiments, jumps in the streamwise velocity fluctuations are observed at $Re = 1792$, 1885, 1718, and 1823 for the 200 μm, 320 μm, 480 μm, and 640 μm microchannels, respectively. These measured transitional Reynolds numbers of 1718–1885 for square microchannels agree very well with the transitional Reynolds numbers of 1800–2000 that Sharp and Adrian reported for round microtubes. Thus, as in the experiments of Sharp and Adrian, no evidence of early transition was observed in the present study. Note that nearly identical transitional Reynolds numbers are obtained if transition is instead defined by a jump in the centerline transverse velocity fluctuations. Using this definition, transition is observed at $Re = 1885$, 1718, and 1823 for the 320 μm, 480 μm, and 640 μm microchannels (the 200 μm microchannel structurally failed at $Re > 1792$, before a jump in the centerline transverse velocity fluctuations could be observed).

As the Reynolds number is increased above transition, increases in both the streamwise and transverse velocity fluctuations are observed. Eventually, the fluctuations no longer increase with increasing Reynolds number, and this behavior, along with the mean velocity profiles approaching that of fully turbulent flow (Fig. 4) is indicative of a fully turbulent state being reached. Observing Fig. 5 once more, it is apparent that the 200 μm microchannel failed before a fully turbulent

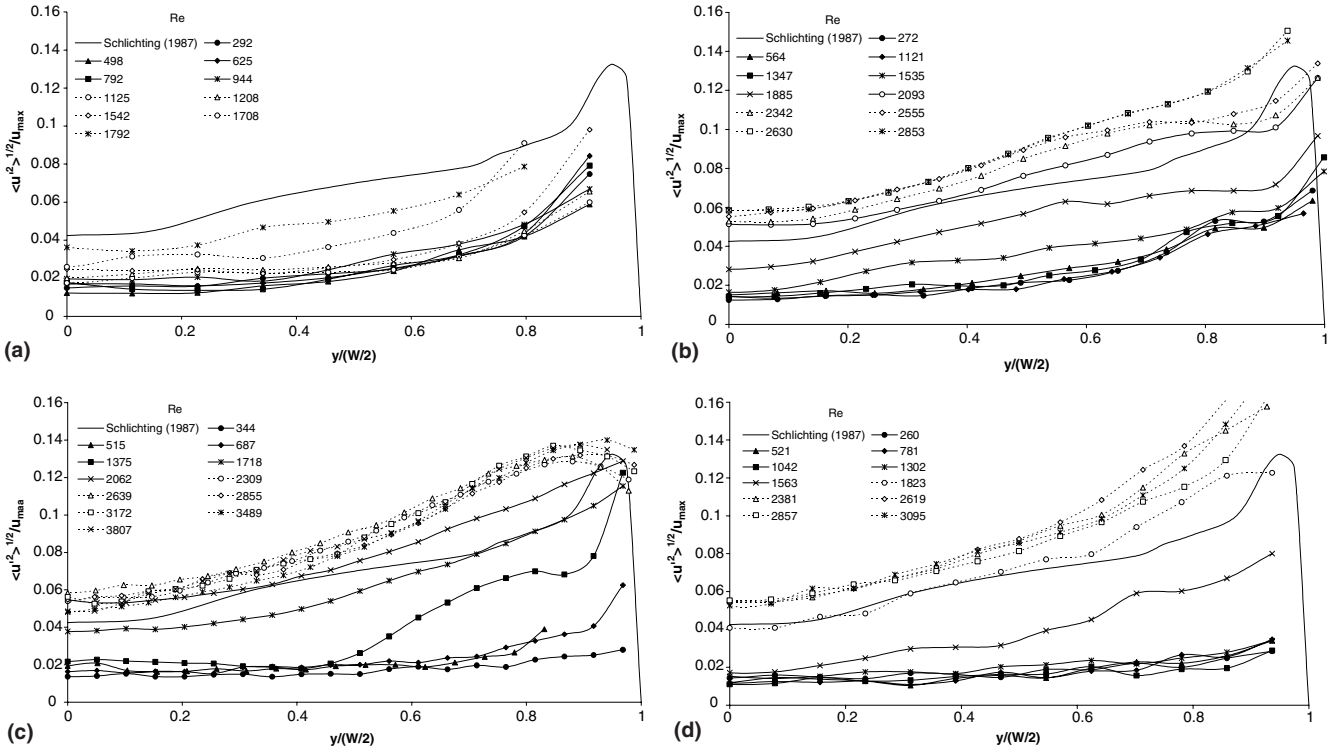

Fig. 5. Streamwise velocity fluctuations for the (a) 200 μm, (b) 320 μm; (c) 480 μm, and (d) 640 μm microchannels.

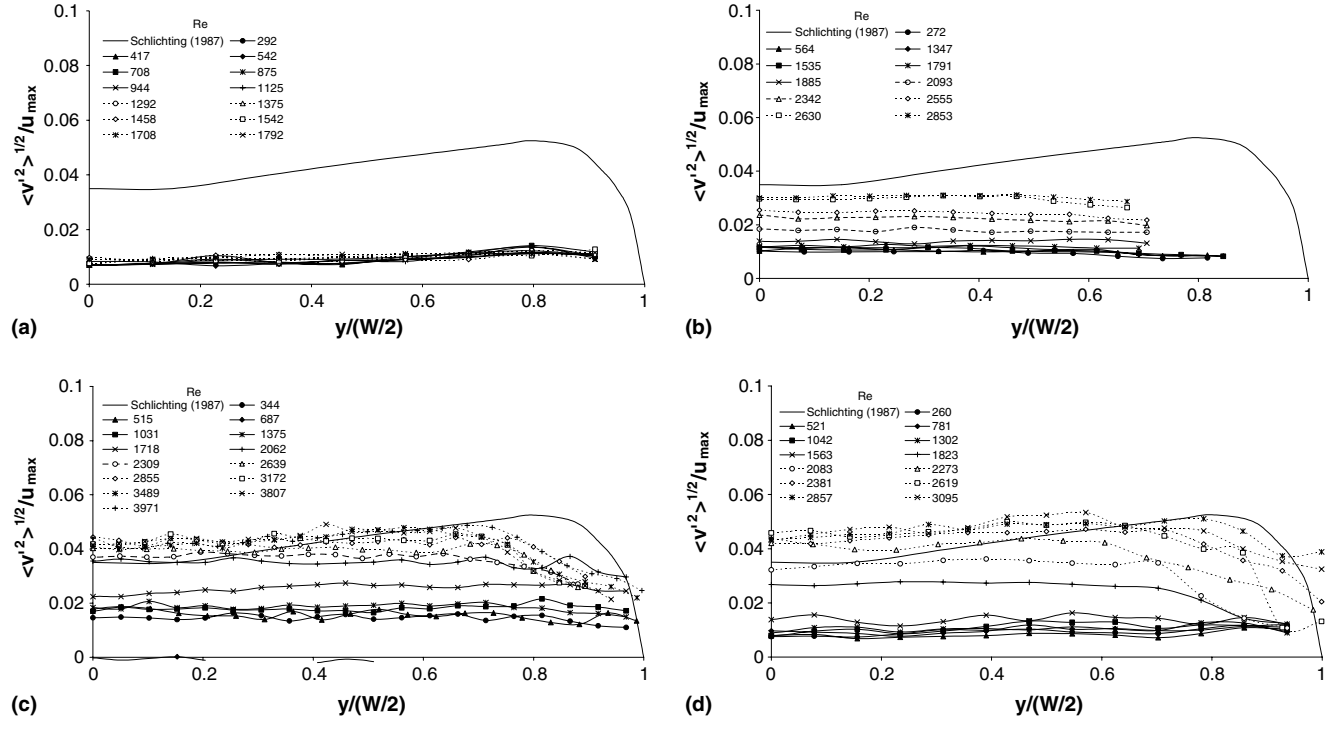

Fig. 6. Transverse velocity fluctuations for the (a) 200 μm, (b) 320 μm; (c) 480 μm, and (d) 640 μm microchannels.

state was reached, since the $Re = 1708$ and $Re = 1792$ results do not overlap. However, fully turbulent flow was observed in the three other microchannel geometries investigated. Both the $\langle u' \rangle / u_{\max}$ and the $\langle v' \rangle / u_{\max}$ fluctuations consistently overlap for the 320 μm, 480 μm, and 640 μm microchannels at Reynolds numbers somewhere

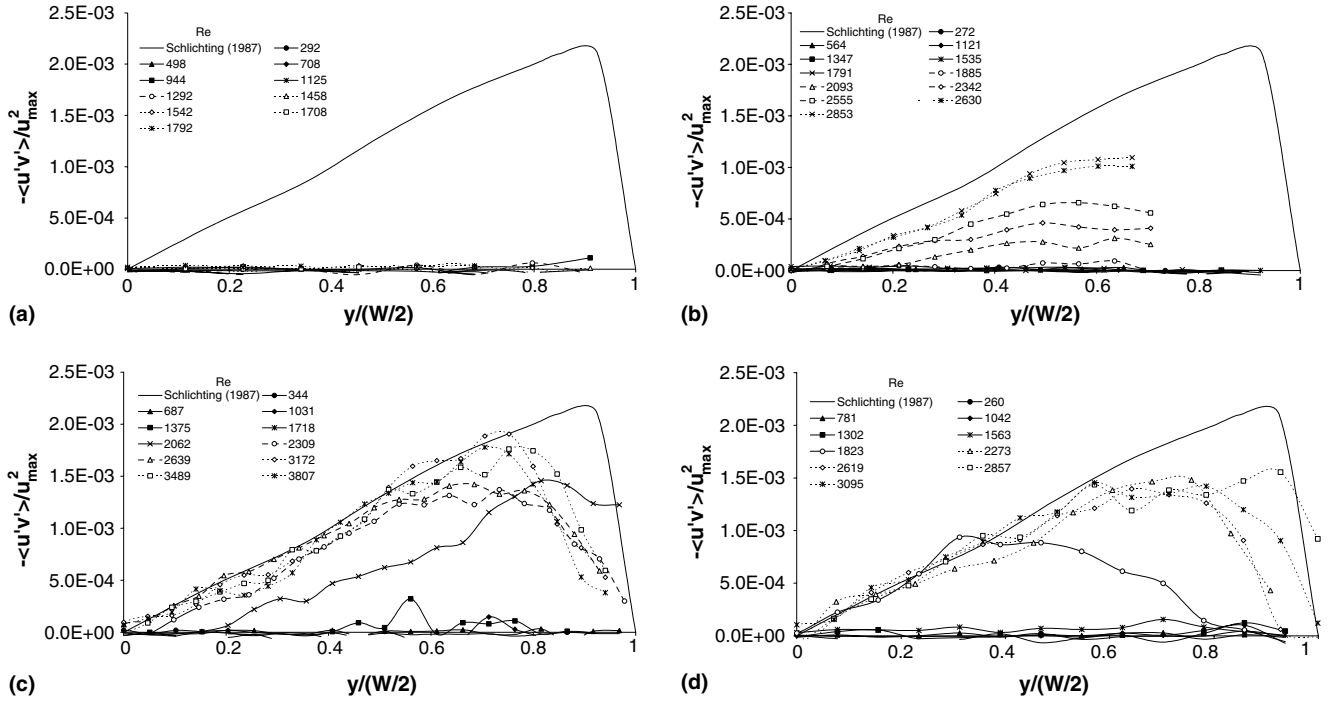

Fig. 7. Reynolds shear stress for the (a) 200 μm, (b) 320 μm; (c) 480 μm, and (d) 640 μm microchannels.

in the range $2400 < Re < 2600$. Coupling these results with the mean velocity profiles shown in Fig. 4 suggest fully turbulent flow being reached in the approximate range of $2600 < Re < 2900$.

The solid lines in Figs. 5 and 6 represent experimental results for turbulent duct flow (Schlichting, 1987). The experimentally determined fully turbulent values for $\langle u' \rangle / u_{\max}$ presented in Fig. 5 are slightly higher than classical results for turbulent duct flow (Schlichting, 1987), but in general, the agreement is good, as all of the results fall within the experimental uncertainty. Similarly, the results of $\langle v' \rangle / u_{\max}$ for the 480 μm and 640 μm microchannels agree very well with the turbulent duct flow results, with the microchannel results slightly higher than the duct flow results over most of the microchannel, but falling within the experimental uncertainty. Although lower $\langle v' \rangle / u_{\max}$ fluctuations are measured near the walls, these results also fall within the experimental uncertainty (note that the measurement uncertainty is higher near the walls because of smaller particle displacements due to lower velocities (Prasad et al., 1992)). The first suggestion of discrepancies between the microchannel results and turbulent duct flow is observed in the measured $\langle v' \rangle / u_{\max}$ fluctuations for the 320 μm microchannel, which are consistently 20–40% lower than the results for turbulent macroscale duct flow.

Fig. 7 shows the Reynolds shear stress, $-\langle u'v' \rangle / u_{\max}^2$, for the four microchannels. In the laminar flow regime, the value of $-\langle u'v' \rangle / u_{\max}^2$ is very close to zero, as expected. For the 200 μm microchannel, $-\langle u'v' \rangle / u_{\max}^2$ is close to zero for all the Reynolds numbers studied. This is not surprising, since the $\langle v' \rangle / u_{\max}$ fluctuations were also seen to be close to zero. For the larger microchannels, as the flow transitions and turbulence become significant, the profiles exhibit a continual increase in value. The value of $-\langle u'v' \rangle / u_{\max}^2$ is nearly zero in the center of the microchannel, as required by symmetry. The peak values in the plot correspond to the locations where the turbulent friction and momentum transportation have their largest values, the locations of highest values of first derivative of $\langle u' \rangle / u_{\max}$ and $\langle v' \rangle / u_{\max}$ fluctuations in Figs. 5 and 6, respectively. The solid lines in Fig. 7 represent the results for fully turbulent macroscale duct flow (Schlichting, 1987). For the 480 μm and 640 μm microchannels (Fig. 7(c) and (d)), an excellent match is observed between the fully turbulent microchannel and macroscale duct flow results over most of the width of the microchannels. There are some discrepancies close to the walls, but as previously stated, measurement errors are higher in these regions. However, for the 320 μm microchannel (Fig. 7(b)), the fully turbulent experimental data of $-\langle u'v' \rangle / u_{\max}^2$ are slightly lower than macroscale turbulent duct flow results.

In addition to providing mean velocity profiles, velocity fluctuations, and Reynolds stress, the microPIV data can also provide information on the large scale turbulent structures present in the flow. One statistical quantity that can be used to describe the turbulent structures is the spatial correlation of velocity fluctuations. The spatial correlations of the u' and v' velocity fluctuations,

$R_{u'u'}$ and $R_{v'v'}$, are calculated using the velocity fluctuations at two locations. For example, $R_{u'u'}$ is calculated as in Eq. (3) below.

$$R_{u'u'} = \frac{\langle u'(0)u'(\Delta y)\rangle}{\sqrt{\langle u'^2(0)\rangle}\sqrt{\langle u'^2(\Delta y)\rangle}} \tag{3}$$

where, $u'(x_0, 0)$ is the streamwise fluctuating velocity component at a point along the channel centerline at streamwise position x_0 , and $u'(x_0, \Delta y)$ is the streamwise fluctuation velocity component at a different transverse position, Δy. The $R_{v'v'}$ correlation is calculated similarly.

The $R_{u'u'}$ and $R_{v'v'}$ spatial correlations in the transverse directions for the 320 μm, 480 μm, and 640 μm microchannels are shown in Figs. 8 and 9, respectively. Since there are no fully turbulent flow data for the 200 μm microchannel, spatial correlation data are not presented for this microchannel. In Fig. 8, $R_{u'u'}$ equals 1 at the channel axis because of the normalization used in Eq. (3). As the correlation distance vector moves away from the channel centerline, $R_{u'u'}$ decreases and exhibits an asymptotic decay to zero at large separation. The correlation coefficients remain positive or converge asymptotically to zero after passing through zero to relatively small negative values. The same trends are seen in the $R_{v'v'}$ correlation, as shown in Fig. 9. In addition to the microchannel data, the correlation function for the streamwise velocity fluctuations in the cross-section of a macroscale circular pipe are also presented for comparison (Taylor, 1936) to demonstrate whether the large structures in the microscale flow exhibit similar behavior to the large structures in a similar macroscale flow. The experimental data for the 480 μm and 640 μm microchannels are seen to agree well with Taylor's results, with the correlation coefficient approaching 0.0 at a distance of approximately 0.4 channel half-widths. However, longer correlation lengths were observed in the 320 μm microchannel than in Taylor's results with the 0.0 value in the correlation coefficient occurring at a distance of approximately 0.9 channel half-widths. The $R_{v'v'}$ correlations decayed slightly more slowly than the $R_{u'u'}$ correlations, and exhibited similar behavior in all three microchannel geometries.

The integral length scale

$$L = \int_0^{W/2} R(y)\mathrm{d}(y) \tag{4}$$

can be used to quantify the characteristic length of large structures in turbulent flow. Table 2 lists the integral length of the spatial correlation functions, $L_{u'u'}$ and $L_{v'v'}$, presented in Figs. 8 and 9 for the 320 μm, 480 μm, and 640 μm microchannels. The $L_{u'u'}$ length scales of the 480 μm and 640 μm microchannels are very close to macroscale value for circular pipe of 0.14, reported by Taylor (1936). The $L_{u'u'}$ length scale for the 320 μm is approximately twice as large, with a value of 0.34. Similar behavior is observed in the $L_{v'v'}$ length scales with the length scales of the 480 μm and 640 μm microchannels similar in value, but with the length scale in the 320 μm being larger.

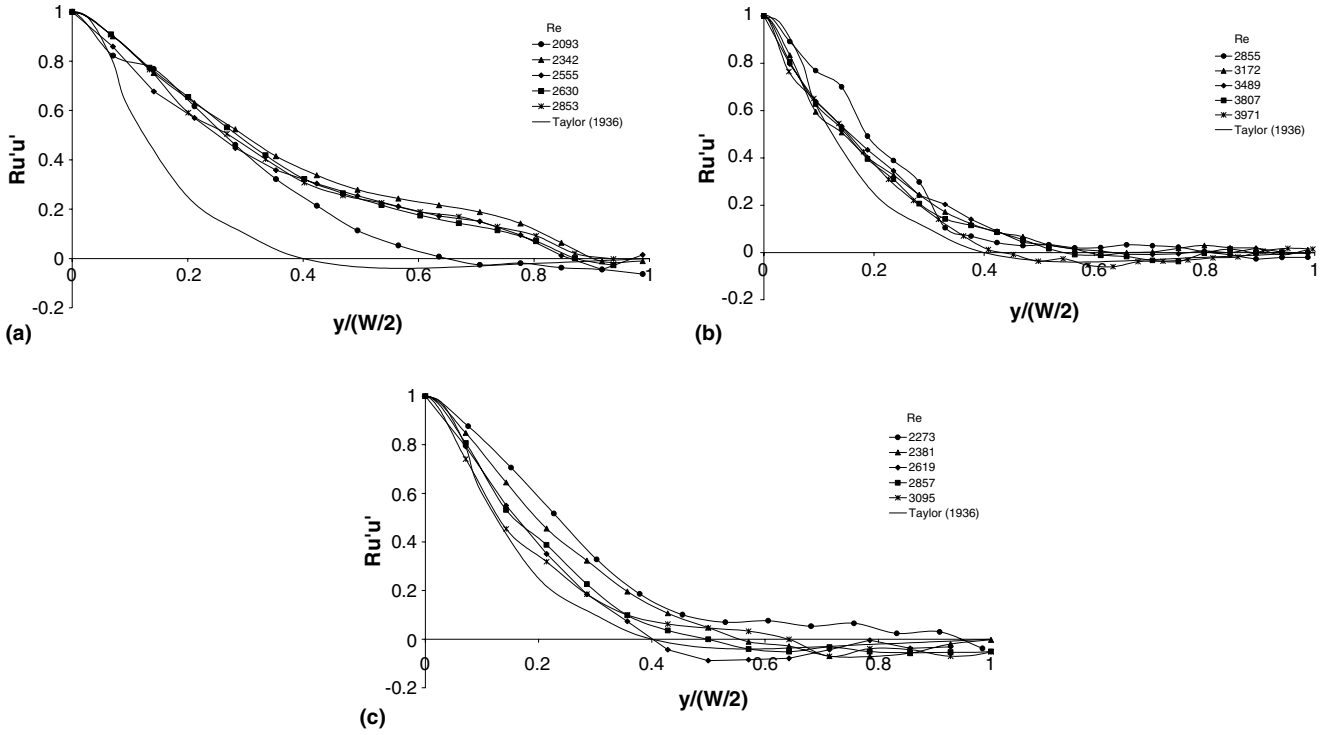

Fig. 8. R_{uu} correlations for the (a) 320 μm; (b) 480 μm, and (c) 640 μm microchannels.

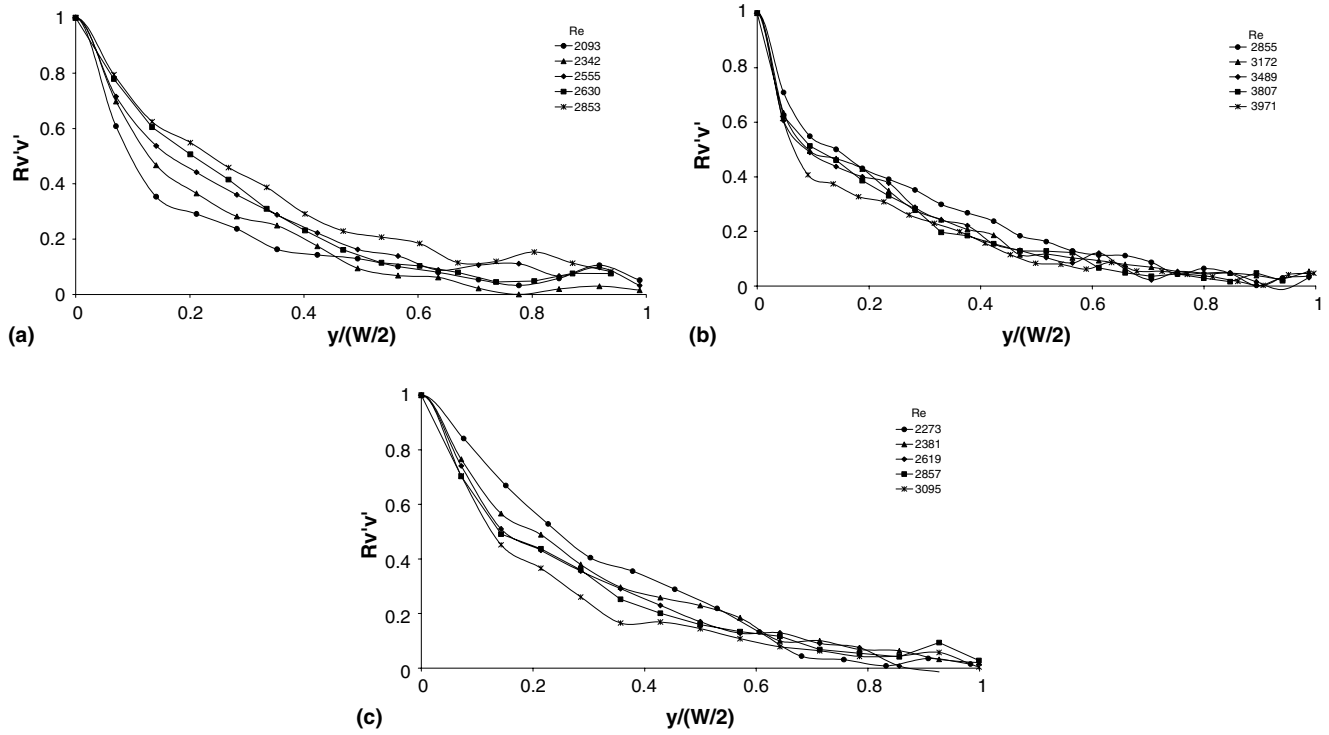

Fig. 9. R_{vv} correlations for the (a) 320 μm; (b) 480 μm, and (c) 640 μm microchannels.

Table 2
Integral length of spatial correlation functions

Channel name	$L_{u'u'}/(W/2)$	$L_{v'v'}/(W/2)$
320 μm	0.34	0.32
480 μm	0.15	0.18
640 μm	0.20	0.20

5. Summary and conclusions

Microscopic particle image velocimetry was used to measure instantaneous velocity fields in square microchannels with hydraulic diameters ranging from 200 μm to 640 μm. Data were collected for Reynolds number ranging from 200 up to 3971. Mean velocity profiles, velocity fluctuations, Reynolds stresses, and spatial correlations of velocity fluctuations were calculated from the microPIV data. With transition to turbulence defined by an increase in the measured centerline velocity fluctuations, transition was observed at Reynolds numbers ranging from 1718 to 1885. These data agree very well with the recent experiments of Sharp and Adrian (2004) in round microtubes in which transition was observed at Reynolds numbers between 1800 and 2000. Thus, no evidence of early transition was observed in the present experiments. The 200 μm microchannel structurally failed before fully turbulent flow could be reached. Fully turbulent flow was observed for the larger microchannels (hydraulic diameters of 320 μm, 480 μm, and 640 μm) at Reynolds numbers ranging from 2600 to 2900.

For the fully turbulent flow in the 320 μm, 480 μm, and 640 μm microchannels, the measured $\langle u' \rangle / u_{\max}$ fluctuation was slightly higher than results for macroscale turbulent duct flow, but in general agreed well with the macroscale results. There was some variation in the $\langle v' \rangle / u_{\max}$ fluctuation results for the microchannels studied. The $\langle v' \rangle / u_{\max}$ fluctuations agreed well with macroscale turbulent duct flow results for the 480 μm and 640 μm microchannels, but were 20–40% smaller than the results for turbulent duct flow in the 320 μm microchannel. Similar results were observed in the measured Reynolds shear stresses, with the 480 μm and 640 μm microchannel results agreeing well with the macroscale results, and the 320 μm microchannel results showing slight discrepancies. In the $R_{u'u'}$ spatial correlation results, the 480 μm and 640 μm microchannel results agreed very well with turbulent pipe flow results, but the 320 μm results showed significant differences. The $R_{v'v'}$ spatial correlations were very similar for all three microchannels, with the $R_{v'v'}$ correlations decaying slightly more slowly than the $R_{u'u'}$ correlations.

Acknowledgment

The work was funded by the National Science Foundation under grant number CTS-0134469.

References

Adrian, R.J., Yao, C.S., 1983. Pulsed laser technique application to liquid and gaseous flows and the scattering power of seed material. Applied Optics 24, 42–52.

Anderson, J.R., Chiu, D.T., Jackman, R.J., Chemiavskaya, O., McDonald, J.C., Wu, H., Whitesides, S.H., Whitesides, G.M., 2000. Fabrication of topologically complex three-dimensional microfluidic systems in PDMS by rapid prototyping. Analytical Chemistry 72, 3158–3164.

Bourdon, C.J., Olsen, M.G., Gorby, A.D., 2004. Validation of analytical solution of depth of correlation in microscopic particle image velocimetry. Measurement Science and Technology 15, 318–327.

Celata, G.P., Cumo, M., Zummo, G., 2004. Thermal-hydraulic characteristics of single-phase flow in capillary pipes. Experimental Thermal and Fluid Science 28, 87–95.

Chung, P.M.-Y., Kawaji, M., Kawahara, A., 2002. Characteristics of single-phase flow in microchannels, American Society of Mechanical Engineers. Fluids Engineering Division 257 (1B), 1219–1228.

Devasenathipathy, S., Santiago, J.G., Wereley, S.T., Meinhart, C.D., Takehara, K., 2003. Particle imaging techniques for microfabricated fluidic systems. Experiments in Fluids 34, 504–514.

Gui, F., Scaringe, R.P., 1995. Enhanced heat transfer in the entrance region of microchannels. In: Proceedings of the 30th Intersociety Energy Conversion Engineering Conference, vol. 2, pp. 289–294.

Guo, Z.Y., Li, Z.X., 2003a. Size effect on microscale single-phase flow and heat transfer. International Journal of Heat and Mass Transfer 46, 149–159.

Guo, Z.Y., Li, Z.X., 2003b. Size effect on single-phase channel flow and heat transfer at microscale. International Journal of Heat and Fluid Flow 24, 284–298.

Hegab, H.E., Bari, A., Ameel, T.A., 2001. Experimental investigation of flow and heat transfer characteristics of R-134a in microchannels, microfluidics and BioMEMS. Proceedings of SPIE 4560, 117–125.

Hegab, H.E., Bari, A., Ameel, T., 2002. Friction and convection studies of R-134a in microchannels within the transition and turbulent flow regimes. Experimental Heat Transfer 15, 245–259.

Henning, A.K., 1998. Microfluidic MEMS. IEEE Aerospace Conference, Snowmass, Colorado, March, p. 4.906.

Jo, B.H., Van Lerverghe, L.M., Motsegood, K.M., Beebe, D.J., 2000. Three-dimensional microchannel fabrication in polydimethylsiloxane (PDMS) elastomer. Journal of Microelectromechanical Systems 9, 76–81.

Judy, J., Maynes, D., Webb, B.W., 2002. Characterization of frictional pressure drop for liquid flows through microchannels. International Journal of Heat and Mass Transfer 45, 3477–3489.

Kim, M.J., Beskok, A., Kihm, K.D., 2002. Electro-osmosis-driven micro-channel flows: a comparative study of microscopic particle image velocimetry measurements and numerical simulations. Experiments in Fluids 33, 170–180.

Klank, H., Goranovic, G., Kutter, J.P., Gjelstrup, H., Michelsen, J., Westergaard, C.H., 2002. PIV measurements in a microfluidic 3D-sheathing structure with three-dimensional flow behaviour. Journal Micromechanics and Microengineering 12, 862–869.

Lee, S.Y., Wereley, S.T., Gui, L., Qu, W., Mudawar, I., 2002. Microchannel flow measurement using micro particle image velocimetry. American Society of Mechanical Engineers, Fluids Engineering Division (Publication) FED 258, 493–500.

Li, H., Ewoldt, R., Olsen, M.G., 2005. Turbulent and transitional velocity measurements in a rectangular microchannel using microscopic particle image velocimetry. Experimental Thermal and Fluid Science 29, 435–446.

Lipman, J., 1999. Microfluidics puts big labs on small chips. EDN Magazine, 79–86.

Mala, G.M., Li, D., 1999. Flow characteristics of water in microtubes. International Journal of Heat and Fluid Flow 20, 142–148.

Meinhart, C.D., Wereley, S.T., Santiago, J.G., 1999. PIV measurements of a microchannel flow. Experiments in Fluids 27, 414–419.

Olsen, M.G., Adrian, R.J., 2000a. Out-of-focus effects on particle image visibility and correlation in microscopic particle image velocimetry. Experiments in Fluids 29, S166–S174.

Olsen, M.G., Adrian, R.J., 2000b. Brownian motion and correlation in particle image velocimetry. Optics and Laser Technology 32, 621–627.

Peng, X.F., Peterson, G.P., 1996. Convective heat transfer and fluid flow friction for water flow in microchannel structures. International Journal of Heat and Mass Transfer 39, 2599–2608.

Peng, X.F., Peterson, G.P., Wang, B.X., 1994. Frictional flow characteristics of water flowing through rectangular microchannels. Experimental Heat Transfer 7, 249–264.

Pfund, D., Rector, D., Shekarriz, A., 2000. Pressure drop measurements in a microchannel. Fluid Mechanics and Transport Phenomena 46 (8), 1496–1507.

Prasad, A.K., Adrian, R.J., Landreth, C.C., Offutt, P.W., 1992. Effect of resolution on the speed and accuracy of particle image velocimetry interrogation. Experiments in Fluids 13, 105–116.

Qu, W., Mudawar, I., 2002. Experimental and numerical study of pressure drop and heat transfer in a single-phase micro-channel heat sink. International Journal of Heat and Mass Transfer 45, 2549–2565.

Qu, W., Mala, G.M., Li, D., 2000. Pressure-driven water flows in trapezoidal silicon microchannels. International Journal of Heat and Mass Transfer 43, 353–364.

Sabry, M.N., 2000. Scale effects on fluid flow and heat transfer in microchannels. IEEE Transactions on Components and Packaging Technologies 23 (3), 562–567.

Santiago, J.G., Wereley, S.T., Meinhart, C.D., Beebe, D.J., Adrian, R.J., 1998. A particle image velocimetry system for microfluidics. Experiments in Fluids 25, 316–319.

Schlichting, H., 1987. Boundary-Layer Theory, seventh ed. McGraw-Hill, New York.

Sharp, K.V., Adrian, R.J., 2004. Transition from laminar to turbulent flow in liquid filled microtubes. Experiments in Fluids 36, 741–747.

Stone, S.W., Meinhart, C.D., Wereley, S.T., 2002. A microfluidic-based nanoscope. Experiments in Fluids 33, 613–619.

Taylor, G.I., 1936. Correlation measurements in turbulent flow through a pipe. Proceedings of the Royal Society A 157, 537–546.

Toh, K.C., Chen, X.Y., Chai, J.C., 2002. Numerical computation of fluid flow and heat transfer in microchannels. International Journal of Heat and Mass Transfer 45, 5133–5141.

Tuckerman, D.B., Pease, R.F., 1981. High-performance heat sinking for VLSI. IEEE Electron Device Letters 2, 126–129.

White, F.M., 1991. Viscous Fluid Flow, second ed. McGraw-Hill, New York.

Wu, H.Y., Cheng, P., 2003. Friction factors in smooth trapezoidal silicon microchannels with different aspect ratios. International Journal of Heat and Mass Transfer 46, 2519–2525.

Wu, P.Y., Little, W.A., 1983. Measurement of friction factor for flow of gases in very fine channels used for micro-miniature Joule–Thompson refrigerators. Cryogenics 23, 273–277.

Wygnanski, I.J., Champagne, F.H., 1973. On transition in a pipe. Part I. The origin of puffs and slugs and the flow in a turbulent slug. Journal of Fluid Mechanics 59, 281–335.

Zeighami, R., Laser, D., Zhou, P., Asheghi, M., Devasenathipathy, S., Kenny, T., Santiago, J., Goodson, K., 2000. Experimental investigation of flow transition in microchannels using micron-resolution particle image velocimetry. In: Thermomechanical Phenomena in Electronic Systems—Proceedings of the Intersociety Conference, vol. 2, pp. 148–153.